Aerosol Science and Technology
Publication details, including instructions for authors and subscription information:
http://www.tandfonline.com/loi/uast20

Filter Material Effects on Particle Absorption Optical Properties

Cary Presser [a] , Joseph M. Conny [a] & Ashot Nazarian [a]
[a] National Institute of Standards and Technology , Gaithersburg , Maryland , USA
Accepted author version posted online: 10 Feb 2014.Published online: 28 Mar 2014.

To cite this article: Cary Presser , Joseph M. Conny & Ashot Nazarian (2014) Filter Material Effects on Particle Absorption Optical Properties, Aerosol Science and Technology, 48:5, 515-529, DOI: 10.1080/02786826.2014.890999

To link to this article: http://dx.doi.org/10.1080/02786826.2014.890999

Aerosol Science and Technology, 48:515–529, 2014
ISSN: 0278-6826 print / 1521-7388 online
DOI: 10.1080/02786826.2014.890999

Filter Material Effects on Particle Absorption Optical Properties

Cary Presser, Joseph M. Conny, and Ashot Nazarian
National Institute of Standards and Technology, Gaithersburg, Maryland, USA

Absorption enhancement and shadowing effects were investigated for nigrosin-laden quartz (fibrous), Teflon (matted), and polycarbonate (membrane) filters in inert surroundings at different sample steady-state temperatures and particle mass loadings. Sample absorptivity was determined using a novel laser-heating technique, which is based on perturbing the sample steady-state temperature and monitoring the thermal response during decay back to steady state, along with a model for thermal energy conservation. In addition, transmissivity measurements were carried out to enable determination of the sample absorption coefficient. The results indicated that the isolated-nigrosin absorption coefficient decreased with steady-state temperature and increased with mass loading and filter pore size. Comparing the absorption coefficient for both the isolated nigrosin and nigrosin-laden filters, indicated that absorption enhancement was most significant for the Teflon filters and least significant for the polycarbonate filters. The effect became more significant as the pore size decreased, steady-state temperature increased, and particle mass loading decreased. The decrease in the isolated-nigrosin, mass-specific absorption cross-section with heavier sample loadings was attributed to shadowing effects.

1. INTRODUCTION

1.1. Filter-Based Particle Absorption Enhancement and Shadowing

Collecting particles on filters is the most widely used technique for atmospheric aerosol sampling, primarily because of its low cost and simplicity (Lodge 1989). The class of filter-based particle absorption techniques include the Aethalometer, (Hansen et al. 1984), integrating-plate (IP)/integrating-sphere photometer (Fry et al. 1992; Hitzenberger 1993; Campbell et al. 1995; Lawless et al. 2004), particle soot absorption photometer, PSAP (Bond et al. 1999), and the continuous soot monitoring system, COSMOS (Kondo et al. 2009; Nakayama et al. 2010). These techniques are based on measuring the light transmission through the particle-coated filter to obtain the absorption coefficient in the Beer–Lambert law (or the extinction coefficient when scattering is considered significant). One important issue discussed extensively in the literature (Clarke 1982; Bohren and Huffman 1983; Campbell et al. 1995; Petzold and Schönlinner 2004; Virkkula et al. 2005; Taha et al. 2007; Cappa et al. 2008) is enhancement of the particle absorption coefficient (often referred to as "absorption enhancement") due to two effects, viz., 1) multiple scattering by the filter substrate and 2) scattering by filter-based nonabsorbing particles. This effect is attributed to absorption of backscattered laser light, which on first pass is not absorbed by the absorbing particles discretely distributed over and embedded within the filter (Clark 1982; Bond et al. 1999). As a result, a substantial increase occurs in the measured particle absorption, which is corrected through instrument calibration. Correction schemes have been developed, which are based on empirical measurements to a reference system such as with PSAP (Moosmüller et al. 2009; Bond et al. 2013), or radiative transfer considerations to compensate for filter surface reflected light (multiple-scattering effect) as with the Aethalometer (Virkkula et al. 2005; Collaud Coen et al. 2010; Virkkula 2010) and multi-angle absorption photometers, MAAP (Hänel 1987; Petzold and Schönlinner 2004; Arnott et al. 2005; Petzold et al. 2005; Moteki et al. 2010).

Several values of the correction factor required to compensate for enhanced absorption effects are reported in the literature. Horvath (1997) found for weakly absorbing aerosols on Nuclepore (polycarbonate) filters that the absorption coefficient was too high by a factor of 2.8, using an integrating plate method. Bond and Bergstrom (2006) report in their review of absorption enhancement effects that under certain conditions this effect can require a correction factor of 3.5 with quartz filters (i.e., to correct laser transmission for absorption enhancement). Weingartner et al. (2003) report an average enhanced absorption of 2.14 and 3.6 with quartz filters and different types of soot, using two different Aethalometers. Schmid et al. (2006) reported an enhancement (attributed to

Received 8 April 2013; accepted 7 January 2014.
Address correspondence to Cary Presser, National Institute of Standards and Technology, 100 Bureau Drive, M/S 8320, Gaithersburg, MD 20899-8320, USA. E-mail: cpresser@nist.gov
Color versions of one or more of the figures in the article can be found online at www.tandfonline.com/uast.

filter multiple scattering) of 5.23 (4.55 if corrected for aerosol scattering) using a 7-wavelength Aethalometer with quartz filters for ambient aerosols collected in the Amazon Basin. Taha et al. (2007) cite work with the integrating plate method (using Teflon and Nuclepore filters) to correct the absorption coefficient for filter multiple scattering (by accounting for the filter thickness and composition) and particle-loading effects.

Another filter-based technique is the thermal-optical analyzer (TOA), which distinguishes elemental carbon (EC) (Petzold et al. 2013) mass from organic carbon (OC) mass in carbonaceous particles collected on quartz-fiber filters through a process of thermal desorption of volatile OC species, OC pyrolysis, and thermal oxidation of all carbon (Chow et al. 1993; Birch and Cary 1996). Before and during the heating process, the attenuation of laser light (typically at 633 nm or 670 nm) by the particles and filter is monitored either by light transmission through the filter (TOT) or light reflection from the filter (Conny et al. 2003). Over the years, studies have tried to elucidate various issues associated with the operation of the TOA (Kirchstetter and Novakov 2007), and in particular absorption enhancement, which influences the determination of OC and EC concentrations during the instrument heating protocol. The apparent instrument absorption coefficient for filter-bound particles has been found to be greater than the absorption coefficient of airborne particles by about a factor of 2 or more (Brinkworth 1972; Sadler et al. 1981; Weingartner et al. 2003). Subramanian et al. (2007) demonstrated with a TOA that the presence of liquid organic matter on fibrous filters can influence the instrument absorption measurements. However, much uncertainty still exists in the magnitude of absorption enhancement. Conny (2007) measured the transmission through two individual particle-laden, quartz-fiber filters and then for the same two filters mounted one upon another in different orientations of the particle-laden surface (i.e., for the coated sides facing upward, downward, and facing one another). Filters coated with particulate matter from different sources were analyzed with a thermal optical transmission instrument. The results indicated that the absorbance for the stacked filters was greater than the sum of the individual filters, and thus an enhancement in absorption was detected of up to a factor of about 1.4. It is also reported (Baumgardner et al. 2012) that using a low-temperature protocol leads to overestimation of the EC, while high-temperature protocols lead to premature evolution of EC. Thus, the sensitivity of the TOA absorption measurements to the heating protocols is not well understood.

Another issue is the effect of the volatile organics on light absorption measurements (Bond et al 2013). Kondo et al. (2011) compared the TOT with a COSMOS system. After heating the COSMOS inlet section to 673 K to remove the volatile compounds, agreement was achieved with the TOT. The BC was cooled before carrying out measurements and monitored to ensure that no recondensation occurred (Kondo et al. 2009). No reason is given as to why the particles are not kept at the inlet temperature during the measurement process. Thus, temperature effects on the absorption measurements and absorption enhancement can potentially be important for these particular instruments.

A third scattering effect is described with regard to the filter particle loading (Weingartner et al. 2003; Arnott et al. 2005; Schmid et al. 2006; Virkkula et al. 2007; Collaud Coen et al. 2010). This opposing effect to absorption enhancement, referred to as "shadowing," occurs for an increased presence of absorbing particles on a filter surface (i.e., with heavier filter mass loading) and results in an apparent reduced optical path length through the coated filter, i.e., an apparent reduction in instrument-reported absorption coefficient (Weingartner et al. 2003; Conny et al. 2009). Also, multiple-scattering effects for absorbing particles embedded within a fibrous filter appear to be obscured by the layer of surface particles (Arnott et al. 2005; Kirchstetter and Novakov 2007). As a result, it is unknown to what extent absorption enhancement and shadowing influence the determination of absorption properties by filter-based techniques (Baumgardner et al. 2012).

1.2. Measuring Filter-Based Particle Absorption by Laser-Heating

In this investigation, a rapid laser-heating approach was used to determine the absorptivity of quartz-fiber (fibrous), Teflon (matted), and polycarbonate (membrane) filters coated with nigrosin (a highly absorbing substance Sedlacek and Lee 2007) over a range of steady-state temperatures. The concept involves heating selected samples to a steady-state temperature, perturbing the temperature with a laser beam that impinges directly on the particles, and monitoring the temperature decay back to the steady state. Substance absorptivity at a given temperature and wavelength was determined using the recorded time-resolved temperatures and a model for thermal energy conservation. Transmissivity measurements were also carried out, along with the absorptivity, to provide the particle absorption coefficient. Measurements for both clean and coated filters enabled determination of the isolated particle absorption characteristics, which (when compared with the coated filters) was used to estimate absorption enhancement effects.

2. EXPERIMENTAL APPROACH

A rapid laser-heating approach, referred to as the laser-driven thermal reactor (LDTR), was used to determine the particle absorptivity for six types of commonly used filters that were coated with nigrosin. The LDTR measures the temporally resolved temperature response due to exothermic/endothermic changes in a substance thermal, chemical, and phase-change energy content. One major advantage of this approach is that the absorption coefficient can be estimated directly without the need for calibration to offset various sensitivities that afflict several of the aforementioned instruments (Moosmüller et al. 2009) (see Presser 2012 for validation of the approach). The LDTR approach measures the filter absorption with and without the sample particles so as to isolate and remove the filter effect from the measurements.

Determination of the absorption coefficient for particle-laden filters (being treated as a bulk material Presser 2012), requires measurement of the sample transmissivity in addition to the LDTR measurement.

2.1. Nigrosin Properties

Nigrosin is a mixture of synthetic black dyes used in making India ink. Its chemical formula is reported as $C_{48}N_9H_{51}$ (molecular weight of 753 g·mol^{-1}) (Bond et al. 1999; Kondo et al. 2009), however, other physical and chemical properties are unavailable. The absorption spectrum for nigrosin is broadband from the visible through the near infrared (Justus et al. 1993a,b; Radney et al. 2009).

2.2. Filter Properties

Samples were prepared by coating commercially available nigrosin on different types of 47-mm diameter filters, (1) PallFlex[1] pure quartz fiber (no binder), (2) Pall Zefluor and Zylon polytetrafluoroethylene (PTFE) Teflon, and (3) Whatman Nuclepore track-etched polycarbonate. The pore diameters were 1 μm for the Zefluor, 5.0 μm for the Zylon, and 1 μm, 5 μm, and 10 μm for the Nuclepore filters. The Teflon filters have nonstraight-through pores while the polycarbonate filters are straight-through pores produced by penetrating nuclear-decay particles (Baker 2004). The full-size membrane was used for the extinctions measurements. The filter samples used for the LDTR experiments were punched (with a stainless steel cylinder sharpened at one end) from the larger coated membranes with a diameter of (5.1 $\pm$ 0.1) mm.[2] The measured filter thickness varied with the filter type: i.e., (635 $\pm$ 3) μm for quartz, (229 $\pm$ 3) μm for Zefluor, (190 $\pm$ 3) μm for Zylon, and (25 $\pm$ 3) μm for each Nuclepore filter. The color of the filters was white for the quartz and Teflon filters, which lend themselves to more surface scattering than the transparent polycarbonate filters.

2.3. LDTR Experimental Arrangement

Schematics of the experimental arrangement for the LDTR absorptivity measurements are provided in the online supplementary information (SI) section along with additional operating details. The transmissivity is measured at atmospheric conditions within the vacuum chamber after modifying the LDTR arrangement.

[1]Certain commercial equipment or materials are identified in this publication to specify adequately the experimental procedure. Such identification does not imply recommendation or endorsement by the National Institute of Standards and Technology, nor does it imply that the materials or equipment are necessarily the best available for this purpose.

[2]Estimation of the measurement uncertainty for this study is determined from statistical analysis of a series of replicated measurements (referred to as Type A evaluation of uncertainty), and from means other than statistical analysis (referred to as Type B evaluation of uncertainty) (Taylor and Kuyatt 1994). The Type A expanded uncertainty is calculated as $k_c u_c$, where k_c is the coverage factor and u_c is the combined standard uncertainty. The value for u_c is estimated statistically by $sn^{-1/2}$, where s is the standard deviation of the mean and n is the number of samples. For $n = 3$ and 5, $k_c = 3.18$ and 2.57, respectively, representing a level of confidence of 95%.

2.4. LDTR Experimental Protocol

The experimental protocol for the absorptivity measurements involves using a high-powered laser (operating in the infrared) to heat a small copper-foil spherical reactor to a selected steady-state temperature. The reactor is positioned near the center of a 5 L vacuum chamber containing five viewing ports (four ports on the chamber side placed 90 degrees apart and one port on the top). Sample is placed on, and in contact with, a fine-wire thermocouple that is positioned near the center of the spherical reactor prior to a measurement. Measurements were carried out in an inert helium environment (same as that for TOA) and under vacuum to prevent sample oxidation. A portion of the laser beam was used for the separate transmissivity measurements.

2.4.1. Coating of the Filters

A simple apparatus was assembled to coat the different filters (see section S1.3 in the SI). The portion of the filter exposed to the particle stream was 35 mm in diameter. The time required for achieving qualitatively the desired particle loading varied with each filter type; i.e., up to 5 min for the quartz, 5 min for the Zefluor, 60 min for the Zylon, and (5, 20, and 40) min for the Nuclepore filters with 1-, 5-, and 10-μm pore size, respectively. More time was required to coat the filters with the larger pore sizes, perhaps due to fewer pores per unit area and particle clogging of the pores. Qualitatively, the filters were coated to vary the particle loading from a visually subjective light (1 mg–3 mg), medium (8 mg–12 mg) to heavy (17 mg–18 mg) coating, depending on the filter type (Table 1). The flow rate (from a rotameter) and pressure drop through the clean filters are also presented in Table 1.

2.4.2. Transmissivity Measurements

Each filter was mounted on a support and placed in the path of a diverted portion of the infrared laser beam. The ratio of the transmitted to incident intensities (i.e., $\tau \equiv I_\tau/I_I$) provided a measure of the transmissivity (τ) for both the clean and coated filters. The filter was fixed in position and did not account for possible coating variations over the filter face. Several readings were recorded and averaged. It was assumed that the transmissivity of a particular filter did not change during the LDTR absorptivity measurements at elevated temperatures.

2.4.3. Absorptivity Measurements

The sample was heated indirectly to a preselected steady-state temperature with the infrared laser beam (which is split into two beams and expanded to near the reactor diameter with concomitant beam steering and attenuation optics) by directing the beam to opposing sides of the reactor surface. This laser beam is referred to as the "heating" beam. The continuous-wave multimode Nd:YAG laser, operating at a wavelength of 1064 nm, was used as the light source for heating the reactor. The laser-beam intensity (directed at the sphere) was controlled by exchanging a pair of spatial apertures within the vacuum chamber, which resulted in achieving six different sample steady-state temperatures per filter (i.e., with apertures of different size). Then direct

TABLE 1
Coating parameters for the different full-size filter materials

Filter type	Flow rate [$cm^3 \cdot s^{-1}$]	Pressure drop [kPa]	Mass loading	Nigrosin mass [g]	Approx. coating time [min]
Quartz (fibrous)	212.4	13.5	Lighter	0.0001	1
			Medium	0.0002	2
			Heavier	0.0003	3
Zefluor (1 μm pore size)	196.6	15	Lighter	0.0001	1–2
			Medium	0.0003	3
			Heavier	0.0005	5
Zylon (5 μm pore size)	180.9	17	Lighter	0.0001	7
			Medium	0.0008	30
			Heavier	0.0015	60
Nuclepore (1 μm pore size)	196.6	15	Lighter	0.0006	2
			Medium	0.0014	3
			Heavier	0.0017	5
Nuclepore (5 μm pore size)	212.4	13.5	Lighter	0.0006	5
			Medium	0.0010	10
			Heavier	0.0018	15
Nuclepore (10 μm pore size)	212.4	13.5	Lighter	0.0007	20
			Medium	0.0013	30
			Heavier	0.0018	40

laser heating of the sample was provided from a third focused beam (referred to as the "probe" beam). Wavelength dependence can be evaluated using any laser, but for this study, a portion of the infrared source beam was diverted through the opening in the top of the spherical reactor. Thus, at the steady-state sample temperature, the probe beam increased the sample temperature to a new perturbation steady-state temperature (of less than 10% of the initial steady-state value). The temperature decay back to the initial steady-state temperature was then monitored after the probe beam was blocked, and the experiment was concluded after disengaging the infrared heating beam. The thermogram (i.e., recorded sample temperature with respect to time) was then analyzed to determine the absorptivity.

3. PARTICLE ABSORPTION - THEORETICAL ANALYSIS

The theoretical model is based on the fact that light absorption is a process dependent on principles of heat transfer, as well as electromagnetism. The theoretical analysis used to determine bulk substance absorptivity involves modeling the equation for thermal energy conservation during laser heating to a given steady-state temperature and the subsequent decay in temperature after laser heating termination (Presser 2012), as outlined above. In addition, transmission of radiation through a plane-parallel portion of an arbitrary homogeneous bulk substance (Siegel and Howell 1981; Bohren and Huffman 1983) is used in conjunction with the absorptivity analysis to determine the substance absorption coefficient. The details are presented in Presser (2012), along with relevant information in the SI.

The analysis results in an expression for the absorption coefficient of the particle-laden substrate (α_{ps}) and isolated particles (α_p). One may then define an absorption enhancement factor (α_R) as

$$\alpha_R \equiv \frac{\alpha_{ps}}{\alpha_p} = \frac{C_{ps}\, m_{ps}}{C_p\, m_p} \ , \qquad [1]$$

where C is the mass-specific absorption cross-section, m is the sample mass, and the subscripts p and s refer to the particle and substrate, respectively. Note, the particle spatial dispersion is considered the same with and without the filter (i.e., the sample geometric cross-sectional area, A, and characteristic path length through the sample, d_c, remain unchanged, see the SI). This expression provides an estimate for the contribution of the substrate scattering to enhancing particle absorption.

3.1. Criteria Regarding the Change in Absorption with Steady-State Temperature

Several criteria must be satisfied to ensure consistency in the measurements, which are specified in the SI section (also Presser 2012). Several additional criteria must be satisfied when considering how the filter absorption characteristics change with increasing steady-state temperature and filter particle loading, as listed in Table 2. Also, certain relationships exist that are dependent on the initial steady-state sample temperature (T_o) and also must be satisfied for each set of experiments (as given in Table 2). An expression is derived (see the SI) for the

TABLE 2
Various relationships that need to be satisfied by the calculated parameters (dT/dt is the decay temperature-time derivative, τ is the transmissivity, ρ is the reflectivity, and β is the absorptivity)

Change with filter case [for a particular loading and spatial aperture]	Change with particle loading [for a particular spatial aperture]	Change with T_o per filter [τ = constant]
n – isolated nigrosin	l – lower loading	lt – lower value of T_o
cf – clean filter	h – higher loading	ht – higher value of T_o
nf – nigrosin-laden filter		
$\lvert dT/dt\rvert_{nf} > \lvert dT/dt\rvert_{cf}$	$\lvert dT/dt\rvert_{nf,h} > \lvert dT/dt\rvert_{nf,l} > \lvert dT/dt\rvert_{cf}$	$\lvert dT/dt\rvert_{lt} > \lvert dT/dt\rvert_{ht}$
$\tau_n > \tau_{cf} > \tau_{nf}$	$\tau_{cf} > \tau_{nf,l} > \tau_{nf,h}$	$\rho_{ht} > \rho_{lt}$
$\rho_{cf} > \rho_{nf} > \rho_n$	$\rho_{cf} > \rho_{nf,l} > \rho_{nf,h}$	$\beta_{lt} > \beta_{ht}$
$\beta_{nf} > \beta_n > \beta_{cf}$	$\beta_{nf,h} > \beta_{nf,l} > \beta_{cf}$	$\alpha_{lt} > \alpha_{ht}$
$\alpha_{nf} > \alpha_n > \alpha_{cf}$	$\alpha_{nf,h} > \alpha_{nf,l} > \alpha_{cf}$	

absorptivity $\beta(T)$, which is given by

$$\beta(T) = \frac{c_p(T_{\max})m\Delta T}{I_I A\tau^*}, \quad [2]$$

where $c_p(T)$ is the specific heat capacity, T is the sample temperature, $T_{\max}$ is the perturbation steady-state sample temperature, ΔT is the temperature difference ($\equiv T_{\max} - T_o$), τ^* is the temperature-dependent relaxation time, and I_I is the incident radiation intensity. The derivative of β with respect to T_o is expressed as

$$\frac{d\beta}{dT_o} = -\frac{c_p(T_{\max})m}{I_I A\tau^*}. \quad [3]$$

Since all terms in Equations (2) and (3) are positive, the change in absorptivity with steady-state temperature will be linear with a negative slope. An expression for the absorption coefficient (α) is derived as

$$\alpha = -\frac{1}{d_c}\ln\left[\frac{\nabla}{I_I A\tau^*(1-\rho)^2}\right], \quad [4]$$

where ρ is the reflectivity ($= 1 - \tau - \beta$), and the derivative with respect to T_o is

$$\frac{d\alpha}{dT_o} = -\frac{c_p(T_{\max})\,m}{d_c\,\nabla}, \quad [5]$$

where $\nabla = I_I A\tau^*(1-\rho) - c_p(T_{\max})\,m\,\Delta T$ and must be a positive number to satisfy the logarithm term in Equation (4). Equations (4) and (5) indicate that the change in the absorption coefficient with steady-state temperature must be positive, logarithmic with a negative slope, i.e., the positive portion of the general relationship $y = -\ln(x)$.

The relaxation time, which is defined in the SI by an assumed exponentially decaying expression that represents the fit to the thermogram, is given as:

$$\tau^*(T) = \frac{t}{\ln\frac{T_{\max}-T_o}{T-T_o}}. \quad [6]$$

Figure 1 illustrates how the terms ΔT, Δt ($= t_o - t_b$), and $[dT/dt]^{T\max}$ change during the perturbation temperature decay. The term t_b is the time corresponding to the onset of the perturbation temperature decay, and t_o is the time at which the decaying sample temperature returns to T_o. The term $[dT/dt]^{T\max}$ is the temperature-time derivative at the onset

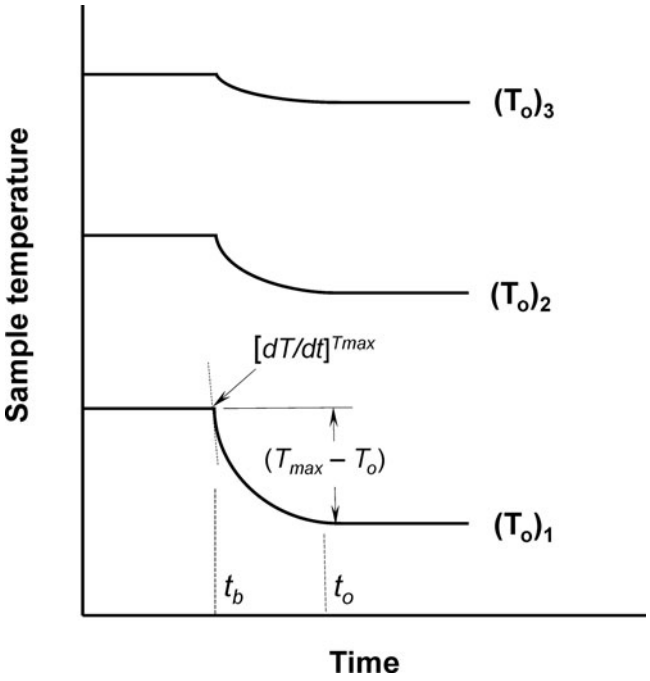

FIG. 1. Illustration of how the terms ΔT ($= T_{\max} - T_o$), Δt ($= t_o - t_b$), and $[dT/dt]^{T\max}$ change during the perturbation temperature decay for a given probe beam power and different values of T_o. The term t_o is the time at which the decaying sample temperature returns to T_o.

of the perturbation temperature decay (i.e., at $T_{\max}$). The magnitude of the negative slope $[dT/dt]^{T\max}$ and the term ΔT decrease with increasing T_o (i.e., different experimental runs) for a given probe beam power, according to the following relationships: $\Delta T_{(T_o)_1} > \Delta T_{(T_o)_2} > \Delta T_{(T_o)_3}$, $\Delta t_1 > \Delta t_2 > \Delta t_3$, and $|dT/dt|^{T_{\max}}_{(T_o)_1} > |dT/dt|^{T_{\max}}_{(T_o)_2} > |dT/dt|^{T_{\max}}_{(T_o)_3}$. This behavior is attributed to the fact that radiative heat transfer to the surroundings is reduced due to the smaller temperature difference between the sample and the surrounding environment (Incropera and DeWitt 2001). According to Nazarian and Presser (2008), $[\tau^*]^{-1}$ increases linearly with increasing T_o (i.e., as the number of experimental runs at different values of T_o is expanded). Thus, the decrease in $[dT/dt]^{T\max}$ and ΔT with increasing T_o (with $d\Delta T/dT_o > d[dT/dt]^{T\max}/dT_o$) must satisfy this criterion. Rearrangement of Equation (6) for the inverse relaxation time, taking its derivative with respect to the steady-state temperature, and choosing a reference value for T along the perturbation decay of $T_r = (T_{\max} + T_o)/2$ with a corresponding reference time $t_r = t(T_r)$, results in $[\tau^*]^{-1} = \ln(2)/t_r$ and

$$\left.\frac{d[\tau^*]^{-1}}{dT_o}\right|_j = \left.\frac{1}{\ln(2)\tau^*\Delta T}\right|_j \qquad j = 1, 2, 3, \ldots, n, \qquad [7]$$

where j represents different experimental runs. This equation indicates that the change in inverse relaxation time with steady-state temperature for all other experimental conditions unchanged will be linear with a positive slope.

4. RESULTS AND DISCUSSION

A variety of filter materials were studied in this investigation including quartz fiber, Teflon with two different pore sizes of 1 μm (Zefluor) and 5 μm (Zylon), and polycarbonate (Nuclepore) with three pore sizes of 1 μm, 5 μm, and 10 μm. Measurements were carried out twice and over a range of steady-state temperatures with clean (reference) and nigrosin-laden filters for each filter type. The reported expanded uncertainties are Type A evaluations, which are estimated by determining the standard uncertainty for the variables, completing a propagation of errors analysis, and combining of uncertainties to provide the expanded uncertainty.

4.1. Features of the Filters and Coatings

The physical features of the coating on the filters were observed and recorded using an optical/digital microscope with objective magnification of 2x, 10x, 20x, and 100x. For the clean filters, the quartz surface appeared to be fibrous, Teflon appeared to have a matted wavy surface, and polycarbonate had a flat membrane surface with discrete holes distributed randomly and some aggregated overlapping holes. The polycarbonate filters with 1-μm pores had a higher density of holes than for the larger 10-μm pore filters, and were more evenly distributed over the filter surface. The transmission through the clean white quartz filter was lower than the other filters and the transparent polycarbonate filters had the highest transmission.

The filters were coated with three different particle mass loadings—qualitatively classified as lighter, medium, and heavier. Visually, the coating on the quartz filters was observed to be uniform (Figure 2a). A fine film of particles did form on the filter-holder screen (Figure 2b) after coating each filter (presumably from small particles transported through the filter), which was removed before coating the next filter. The Teflon filter coatings contained discrete points, and the polycarbonate filter coatings contained blotchy regions. Under the microscope, the particles on the quartz filters adhered to the fibers near and below the surface. For the Teflon filters, the particles appeared to be distributed discretely over the uneven topography of the matted surface, with regions of larger aggregated particles and other lower-lying regions with apparently few particles. The presence of striations was attributed to the matted surface. However, when the microscope focus was changed over these apparently low-density regions, particle density appeared to be higher in the lower-lying portions of the surface. For the polycarbonate filters, the lighter particle mass loadings sometimes resulted in an observed uniform coating; however, the higher mass loading filters always had blotchy surfaces. Under the microscope, well-defined black spots were observed, which were attributed to particles accumulated at and clogging the filter pores. For the 1-μm pore filters, a checkered pattern (Figure 2a) was observed, presumably related to the flow drawn through the perforated filter-holder screen that resulted in a similar checkered pattern. Under high magnification, the particles appeared to accumulate around the edge of the filter pores (Sadler et al. 1981) and adhered less so to the surface region between the pores. For the 10-μm pore filters, well-defined, larger-diameter black disks were distributed in an aggregated fashion, again corresponding to the clogged filter pores. There was no indication of the screen pattern because the larger holes were not distributed as densely as the smaller 1-μm pore filters, however, the presence of the back plate may have contributed to clogging of pores. The blotchy areas on the filter surface corresponded to the smaller particles coating the filter surface unevenly between the clogged pores.

Scanning electron microscope images of the particle accumulation at the 10-μm polycarbonate filter pores is presented in Figure 3a (lighter coating), for which some of the pores are completely covered with particles and others are not. A higher resolution image of a partially clogged pore is shown in Figure 3b with aggregated particles inside the pore, adhering to and extending away from the pore wall. A clogged pore image is presented in Figure 3c with the presence of fibrous strands, which are also presumed to be nigrosin. Figures 3d and e present images of the 1-μm polycarbonate filter pores from one light (between screen holes) and dark (at the screen hole) region of the checkered pattern (Figure 2a), respectively. It is clear that the dark region has a higher concentration of particles, which are drawn there by the flow through the holes in the perforated screen. The presence of clustered filter pores is also clearly shown in Figure 3d. One can obtain an estimate of

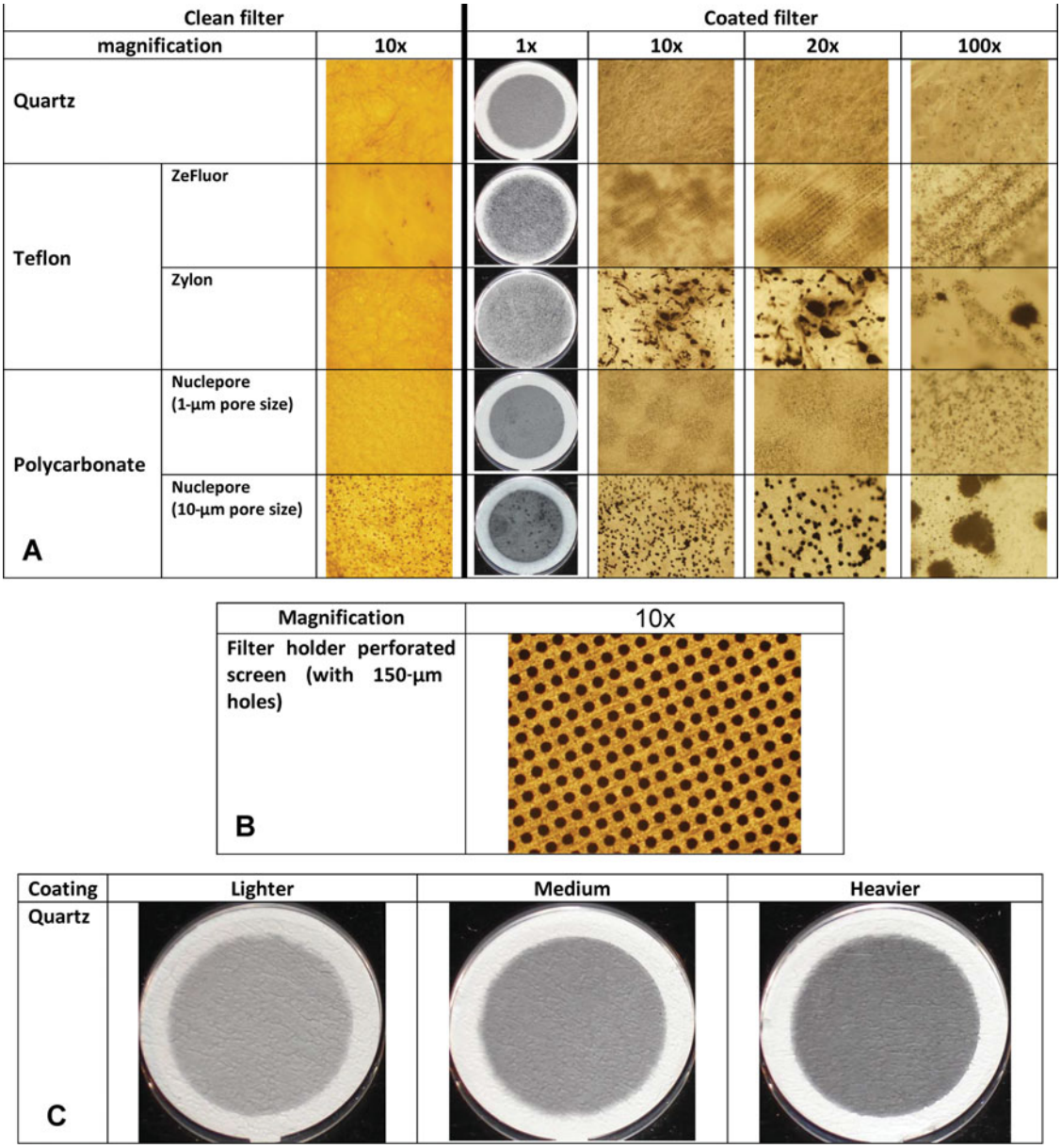

FIG. 2. Photographic images of the (a) particle-laden filters recorded at different microscope magnifications, (b) filter housing back plate, and (c) quartz filters for different particle mass loadings.

the particle sizes by comparing the pore size to the collected particles.

The variation in the particle mass loading is illustrated in Figure 2c for the quartz filter. The filters were coated for a period of time that simulated a qualitatively observed darkening of the filter surface; similar to those collected from atmospheric sampling (thus, highly dense particle loadings were not of interest). The filters were weighed before, during, and after the coating process to estimate the particle mass on the filter. Table 1 presents the measured nigrosin mass on the filters and coating times, as well as the clean filter flow rate and pressure drop. The data in Table 1 indicate that the particle-collection time and measured change in mass varied significantly, although the coating for the different filters was visually similar. The quartz took the shortest time to coat (having a higher flow rate and lower pressure drop than the Teflon filters) and the Zylon took the longest, indicating that the fibrous filters have less of a tendency to clog than the porous filters. The circuitous path through the quartz filter also makes them more efficient at collecting particles. Similarly, coating times increased for the larger pore size filters (e.g., compare the three Nuclepore filters).

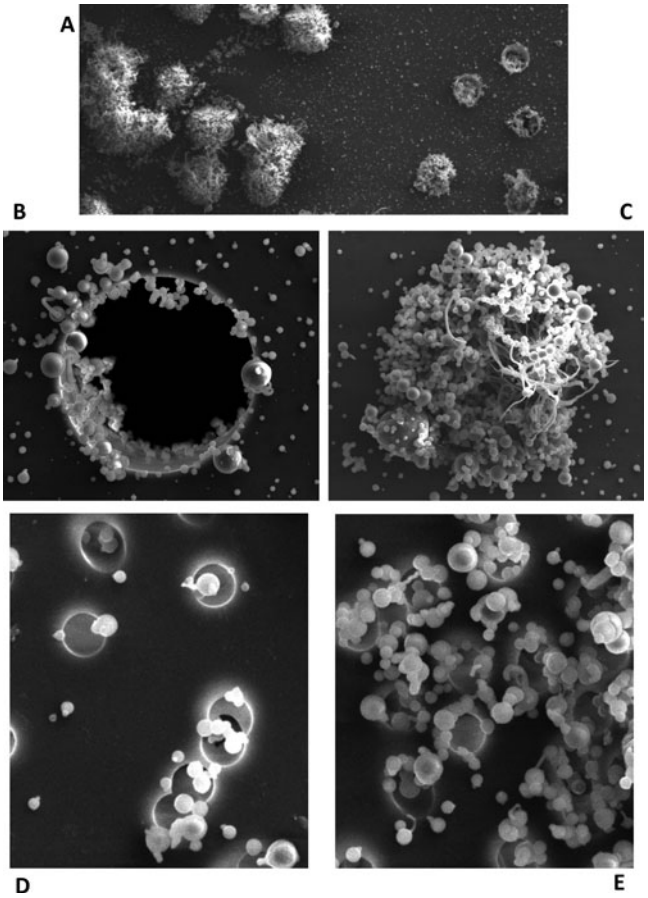

FIG. 3. Field-emission scanning electron microscope image of nigrosin particles on the polycarbonate filters (for all images: lighter nigrosin coating, electron beam energy: 5 kV, current: 25 pA, pixel size [nm]: HFW/1024 horizontal pixels (HFW - horizontal field width), secondary-electron mode, and Everhart–Thornley detector). The filter pore size (FPS), magnification (M), and HFW for each respective image are: (a) FPS: 10 μm, M: 500 x, HFW: 256.0 μm; (b) FPS: 10 μm, M: 8000 x, HFW: 16.0 μm; (c) FPS: 10 μm, M: 6500 x, HFW: 19.7 μm; (d) FPS: 1 μm, M: 8000 x, HFW: 16.0 μm; (e) FPS: 1 μm, M: 8000 x, HFW: 16.0 μm.

4.2. Change in Particle Absorption Characteristics with Steady-State Temperature and Mass Loading

The nigrosin absorption coefficient (α_n) and mass-specific absorption cross-section (C_n) are presented in Figures 4–7 with respect to steady-state temperature (T_o) for the different filter materials and nigrosin mass loadings. Note that Lorenz–Mie theory computations (for an idealized polydispersion of nonaggregated, spherical nigrosin particles well-dispersed within a volume comparable to that of the filter) were found to compare favorably with the experimentally derived absorption coefficient for a nigrosin-laden quartz filter at ambient temperature (Presser 2012). The results in Figures 4–7 are presented for steady-state temperatures up to about 700 K. The melting temperature for quartz is about 1900 K, Teflon (PTFE) is 600 K, and polycarbonate is 413 K. The melting point for nigrosin is about 550 K. After the six temperature runs, the quartz filter appeared unchanged, the Teflon filters kept the coating but were folded after

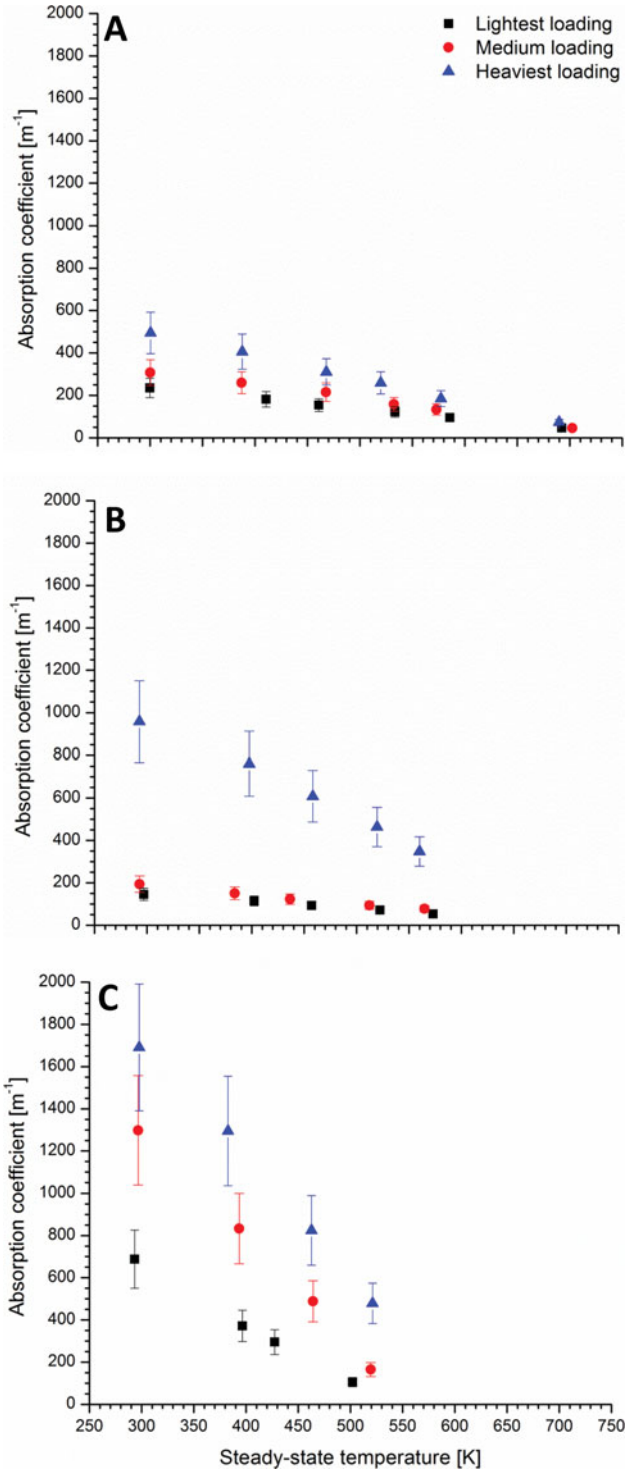

FIG. 4. Variation of isolated-nigrosin absorption coefficient (α_n) with steady-state sample temperature (T_o) at different particle mass loadings for (a) quartz, (b) Zefluor, and (c) Zylon filter materials.

the highest temperature run, and the polycarbonate filters were destroyed after using the fourth spatial aperture.

The general trends regarding the mass loading indicated that the absorption coefficient increased with the mass loading due to the increased absorption (Figures 4 and 5). The mass-specific

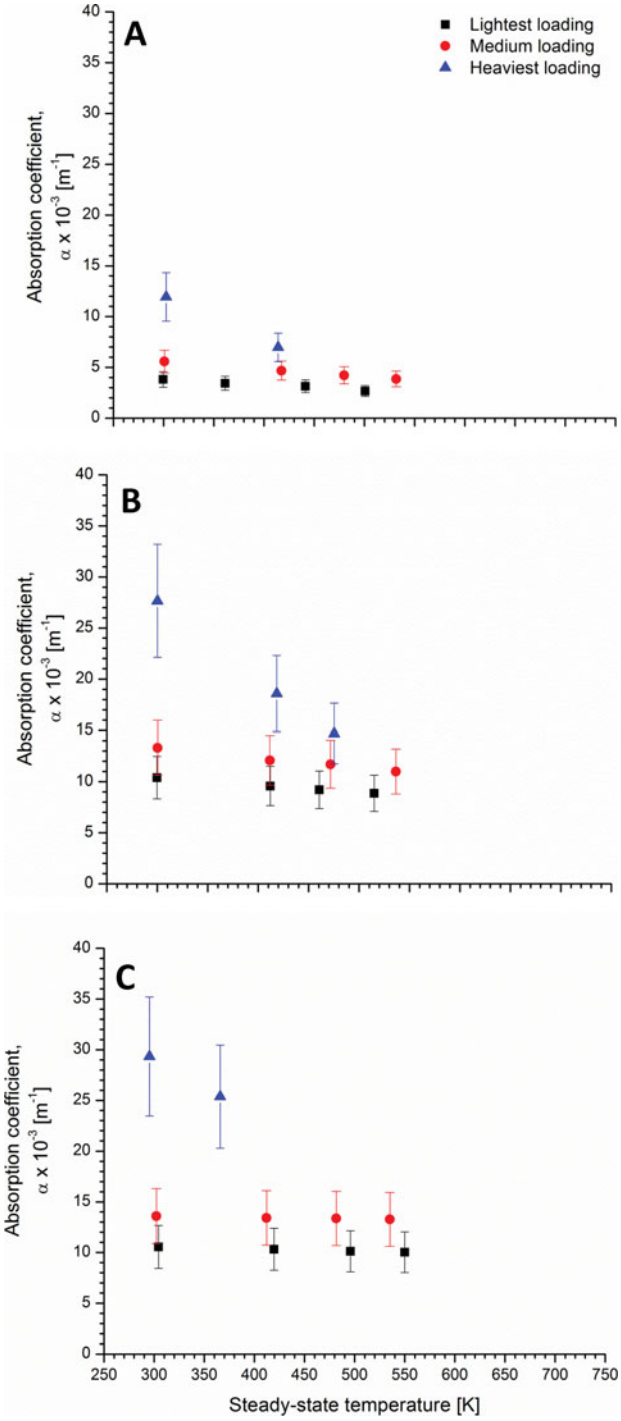

FIG. 5. Variation of isolated-nigrosin absorption coefficient (α_n) with steady-state sample temperature (T_o) at different particle mass loadings for Nuclepore filter materials with (a) 1 μm, (b) 5 μm, and (c) 10 μm pore sizes.

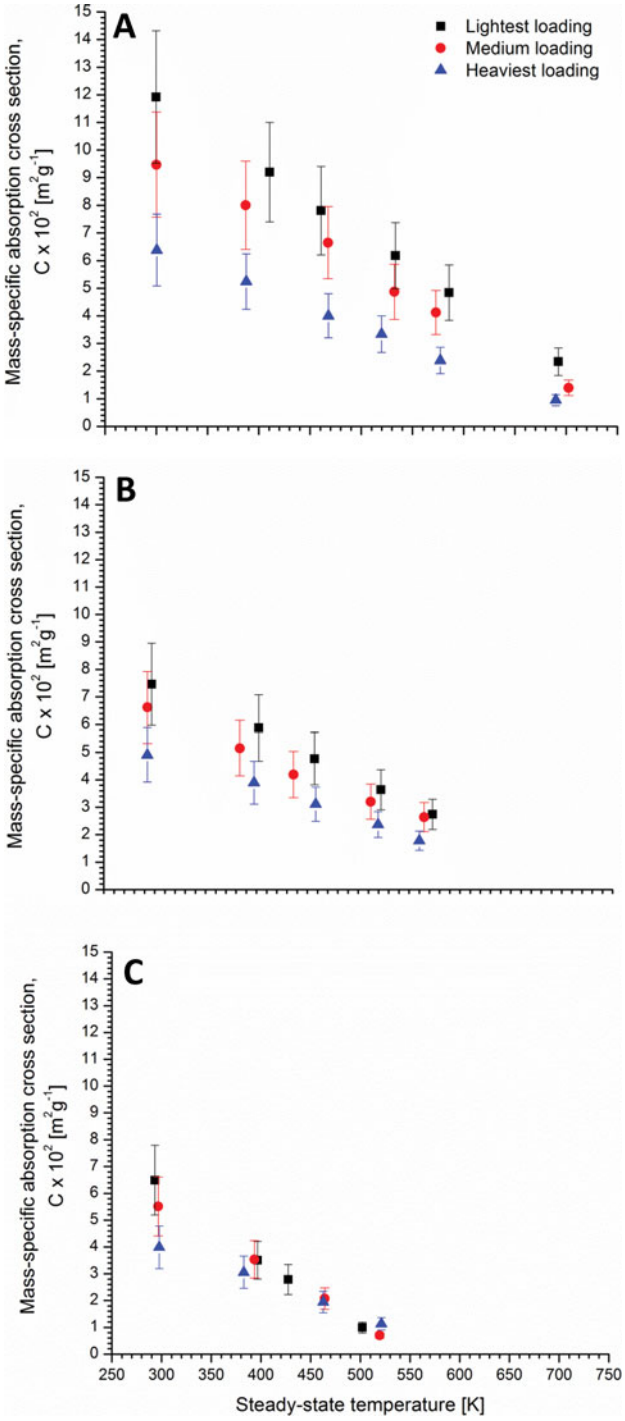

FIG. 6. Variation of isolated-nigrosin, mass-specific absorption cross-section (C_n) with steady-state sample temperature (T_o) at different particle mass loadings for (a) quartz, (b) Zefluor, and (c) Zylon filter materials.

absorption cross-section, C_n, for isolated nigrosin is presented in Figures 6 and 7 and the results indicate a decrease with increased mass loading. Since the value of C_n is an intensive property (i.e., normalized with respect to mass), it would be expected to be independent of the mass loading. However, as mentioned earlier, shadowing effects can alter these results due to particle obscuration by other particles, which would result in reduced absorption for heavier loadings. Thus, as the accumulation of nigrosin increases on the filter surface and in the open areas of the filter shadowing effects become more prominent

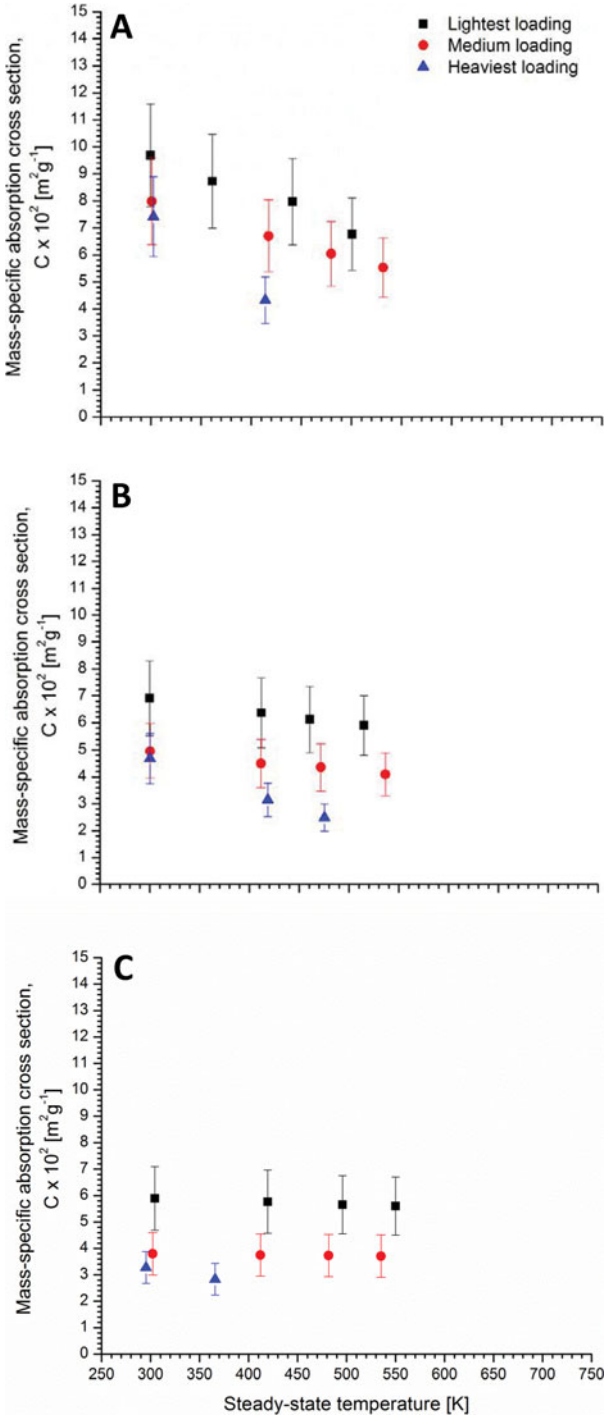

FIG. 7. Variation of isolated-nigrosin, mass-specific absorption cross-section (C_n) with steady-state sample temperature (T_o) at different particle mass loadings for Nuclepore filter materials with (a) 1 μm, (b) 5 μm, and (c) 10 μm pore sizes.

(Sadler et al. 1981; Weingartner et al. 2003; Arnot et al. 2005; Kirchstetter and Novakov 2007; Conny et al. 2009). For example, nigrosin clogs the pores of the polycarbonate filters (Figure 3b) more readily with increased mass loading, which can result in the outer-layer aggregation of particles obscuring those particles within the clogged pore. This causes shadowing effects to become substantial and results in a reduced absorption cross-section. This effect is enhanced with increased filter pore size (the value of C_n decreases by nearly a factor of two when the 10-μm pore size nuclepore filter is compared to the 1-μm pore size filter; Figure 7). This pore-size dependency was also found for the Teflon filters (Figure 6). Similar effects occur for the quartz fibrous filter for which the increased presence of particles on the filter surface obscure light from reaching the particles embedded in the fibers (Kirchstetter and Novakov 2007).

The absorption coefficient generally decreased with increased steady-state sample temperature, as explained by the negative logarithmic trend of Equations (4) and (5). The physical source of this trend relates, as mentioned earlier, to the smaller temperature difference between the sample and surrounding environment at higher steady-state temperatures (Figure 1). Another explanation may be attributed to pyrolysis of the coating on the filter that ultimately resembles the clean filter. However, the visual evidence (i.e., the coating was observed to be similar to the pretest sample) and absence of change in the filter mass (comparing the filter mass before and after the experiments) did not support this possibility. Also, there were no unusual temperature digressions that would be indicative of chemical reaction (Nazarian and Presser 2008). Although efforts were made to ensure that the three mass loadings would be different, one case for the Zefluor resulted in two similar lighter mass loadings (Figure 4b).

Comparison of the different filter types indicated that the relative magnitude of the absorption coefficient at the lower steady-state temperatures was most likely a result of the filter mass loading and pore size. The value of α_n for the quartz filter appears to be smaller than that for the two Telfon filters. The values of α_n for the Zylon filter are generally higher than that for the Zefluor filter (at the lower steady-state temperatures), indicating that absorption increases as the filter pore size increases (1 μm for the Zefluor filter and 5 μm for the Zylon filter). The absorption coefficient for the 5-μm and 10-μm polycarbonate filters (Figure 5) was much larger than for the quartz and Teflon filters. The trend between the polycarbonate filters (with pore sizes of 1 μm, 5 μm, and 10 μm, respectively) was similar to that for the Teflon filters, namely, the value of α_n increased as the pore size increased.

4.2.1. Discussion and Comparison to Literature Results

As described earlier, the operating protocol for filter-based absorption techniques (i.e., for IP, Aethalometer, PSAP and MAAP) relies on measurement of both the transmission and scattering (and estimation of the respective extinction and scattering coefficients). The difference between these two measurements is used to estimate the absorption coefficient. When absorption is small, the difference between two large numbers can lead to inaccuracies due to the presence of the filter material (being more significant for lighter particle loadings) (Bond

et al. 1999). The aforementioned studies listed in the *Introduction* summarize the effect of absorption enhancement (i.e., due to particle-related scattering and filter-matrix multiple scattering effects) and shadowing (i.e., due to filter particle loading). A variety of correction schemes have been developed to account for these scattering effects when referenced to other techniques. For example, Bond et al. (1999) compensates PSAP absorption enhancement effects by comparing the absorption coefficient to that of an IP. The IP is considered a reference system because a diffuse light source is used to remove the filter multiple-scattering effects by index of refraction matching. Petzold et al. (2005), expand on this concept for the MAAP response characteristics by applying the two-stream approximation radiative transfer scheme (Hänel 1994) to model the multiscattering effects. Hänel (1987, 1994) used a polar photometer method to determine the volume scattering and transmission (and subsequently the absorption coefficient) from Nuclepore filters (comparing particle-laden and clean filters). An inversion scheme was developed to better estimate (as compared to earlier investigations) the particle volume scattering. Although a data correction is not required (as with PSAP and Aethalometer data), the inversion process is based on providing initial values for the particle optical thickness or single-scattering parameter. A correction factor is required in order for the inversion process to reduce the uncertainty of the optical parameters when the filter particle loading is too low or high. There is no discussion as to the source of the discrepancy, i.e., regarding absorption enhancement and shadowing. Similarly, the reference measurement used by Petzold et al. (2005) was defined by the transmission (Virkkula et al. 2005) and scattering from an integrating nephelometer. Sheridan et al. (2005) referenced various filter-based instruments to nonfilter-based photoacoustic spectroscopy and cavity ring-down spectroscopy systems.

Regarding shadowing, a correction scheme for filter loading effects was developed for the PSAP (Bond et al. 1999; Sheridan et al. 2005; Virkkula et al. 2005). Collaud Coen et al. (2010) develop a correction scheme, which also included the effects of filter loading for the Aethalometer, based on the earlier work by Weingartner et al. (2003), Arnott et al. (2005), Schmid et al. (2006), Virkkula et al. (2007), and Virkkula (2010). Also note that wavelength corrections (having a power-law dependency) have been used to account for the different instrument laser light sources (Bond et al. 1999; Collaud Coen et al. 2010; Ogren 2010). Again, these corrections are applied to obtain a more precise determination of filter transmission and scattering, so as to improve the estimation of the absorption coefficient.

For this investigation, there are no restrictions due to particle loading (Presser 2012). Comparing the absorption coefficient for Nuclepore filters, the values cited by Hänel (1994) and others are much smaller than reported in this study. This discrepancy is attributed to the definition of the characteristic path length. The measurements by Hänel (1994) are based on a volumetric absorption coefficient, for which the characteristic path length is defined by the column of air drawn through the filter (ratio of the sampling volume to filter cross-sectional area), whereby the characteristic path length for this work was the filter thickness (Bohren and Huffman 1983). Note that for the volumetric representation, an underestimation of the sampling volume is possible if the particle concentration increases within the flow field for a particular particle loading (absorbance), air flow rate, and filter cross-sectional area. Agreement is fine when the absorption coefficient is derived using a characteristic path length that is based on the volumetric flow rate and particle collection time during the filter coating process, and the filter cross-sectional area exposed to the particles (i.e., punch diameter of 5.1 mm). Note that the air flow rates and particle collection times for the full-size filters (Table 1) do not scale linearly down to the punched case, thus requiring separate determination of the sampling volume for the punched specimen. For example, the quartz-filter absorption coefficient (lightest loading, at ambient temperature, volume flow rate of 300 cm^3 min^{-1}, and collection time of 60 min) changes from a value of about 235.3 m^{-1} (Figure 4a) to about 169.5 Mm^{-1}, which is similar to the values given by Hänel (1994) and others using nigrosin-laden glass fiber/cellulose filters (Bond et al. 1999; Sedlacek and Lee 2007; Cappa et al. 2008; Kondo et al. 2009). Virkkula et al. (2005) used atmospheric aerosol and reported results that were similar to that of nigrosin absorption coefficient by Bond et al. (1999). Lack et al. (2006) also report similar values for the nigrosin absorption coefficient using photoacoustic absorption spectroscopy (no filter). Weingartner et al. (2003) presents the absorption coefficients with respect to wavelength for different types of soot on fibrous filters from a spectrum Aethalometer. The absorption coefficient is found to decrease nonlinearly with increasing wavelength, with values of the same order as reported above for this investigation at $\lambda =$ 1064 nm.

Regarding the mass-specific absorption cross-section, Hitzenberger et al. (1996) analyzed black carbon collected on polycarbonate filters over Vienna, Austria, using an integrating sphere and reported values of $C = 10\ m^2\ g^{-1}$ at $\lambda = 550$ nm. Petzold and Schönlinner (2004) used the analysis by Hänel (1994) for a MAAP system to analyze fibrous filters. The absorption coefficient for black carbon urban aerosol was calibrated against Aethalometer measurements, and reported values of $C = 9.1\ m^2\ g^{-1}$ to $10.7\ m^2\ g^{-1}$ at $\lambda = 550$ nm. Fuller et al. (1999) reported that, based on modeling of aggregates of graphitic carbon grains, the value of $C = 10\ m^2\ g^{-1}$ is an overestimation and that light-absorbing carbon in diesel soot is often less than $7\ m^2\ g^{-1}$ at $\lambda = 550$ nm. They also cite other studies for which $C = 5\ m^2\ g^{-1}$ at $\lambda = 685$ nm (black carbon) (Moosmüller et al. 1998) and $4.6\ m^2\ g^{-1}$ at $\lambda = 550$ nm (diesel soot) (Bruce et al. 1991), using photoacoustic systems (no filter). Bond et al. (1999) obtained PSAP results for nigrosin-laden Nuclepore filters with $C = 3\ m^2\ g^{-1}$ at $\lambda = 550$ nm. Similar results are also reported by Mogo et al. (2005) for 1 μm particulate matter on polycarbonate filters using an integrating plate. Taha et al. (2007) measured a value of $C = 1.5\ m^2\ g^{-1}$ at $\lambda = 633$ nm (for crushed graphite carbon on Teflon filters) using a laser integrating-plate

method, and considered the values reported by Hitzenberger et al. (1996) too high. They also report that Nuclepore filters resulted in slightly higher values than those of the Teflon filters. In this light, results for the polycarbonate filters of the current investigation (Figure 7) at ambient temperature are about $C = 0.05$ m^2 g^{-1} to 0.1 m^2 g^{-1} (depending on the filter pore size), which are consistent with Taha et al. (2007) when accounting for the longer wavelength of $\lambda = 1064$ nm (i.e., absorption decreases at longer wavelengths [Moosmüller et al. 1998]). Also, Bruce et al. (1991) reported a mean value of about $C = 0.85$ m^2 g^{-1} for diesel soot in the infrared, which is similar in magnitude to the current investigation.

4.3. Absorption Enhancement and Shadowing Effects

For the aforementioned referenced literature, different empirically derived correction schemes are used to compensate for scattering effects on absorption. With the LDTR approach, the absorption characteristics are determined directly from thermal energy conservation and a model for the transmission of radiation. Considered in the theoretical analysis are the issues of multiple scattering within the filter and surface reflection due to the filter surface or particles (particle scattering in this study is small since nigrosin is essentially absorbing). The analysis also directly considers the absorption through the material and thus accounts for high particle mass loadings (Presser 2012). The effect of the filter is removed from both the absorptivity and transmissivity so as to isolate the absorption by the particles. Secondary effects may be present due to the coupled particle-filter system; however, these effects are estimated to be negligible. The absorption coefficient for the isolated nigrosin is representative of the particles without multiple-scattering effects, which is compared to the nigrosin-laden filter to evaluate the effect of the filter.

One can estimate the absorption enhancement effect of the filter material by comparing the nigrosin-laden filter results to the isolated nigrosin case. The variation of the sample absorption enhancement ratio (α_R, as defined by Equation (1)) with steady-state temperature is presented for the different filter materials and mass loadings in Figures 8 and 9. The results indicate that generally the value of α_R increases as the mass loading decreases and as the value of T_o increases. For the heavier-loaded quartz filter at room temperature, the results are similar to our earlier investigation (Presser 2012). The values of α_R for the quartz and Teflon filters become large for increasing steady-state temperature (Figure 8), and perhaps unreasonable when compared to the literature values reported above in the *Introduction* (e.g., by about a factor 4–5 when comparing fibrous filters at ambient temperature; Figure 8a), but the results for the polycarbonate filters compare well with the above-mentioned literature values (Figure 9). The increase in the value of α_R with lower mass loading is consistent with the increased exposure of the filter material, greater surface scattering, and enhanced absorption effects (Horvath 1993; Kirchstetter and Novakov 2007). Likewise, the influence of the filter substrate is reduced for the heavier mass loadings that may be attributed to shadowing effects (Clarke 1982; Arnott et al. 2005). Similarly, the dependence of the sample absorption enhancement ratio on

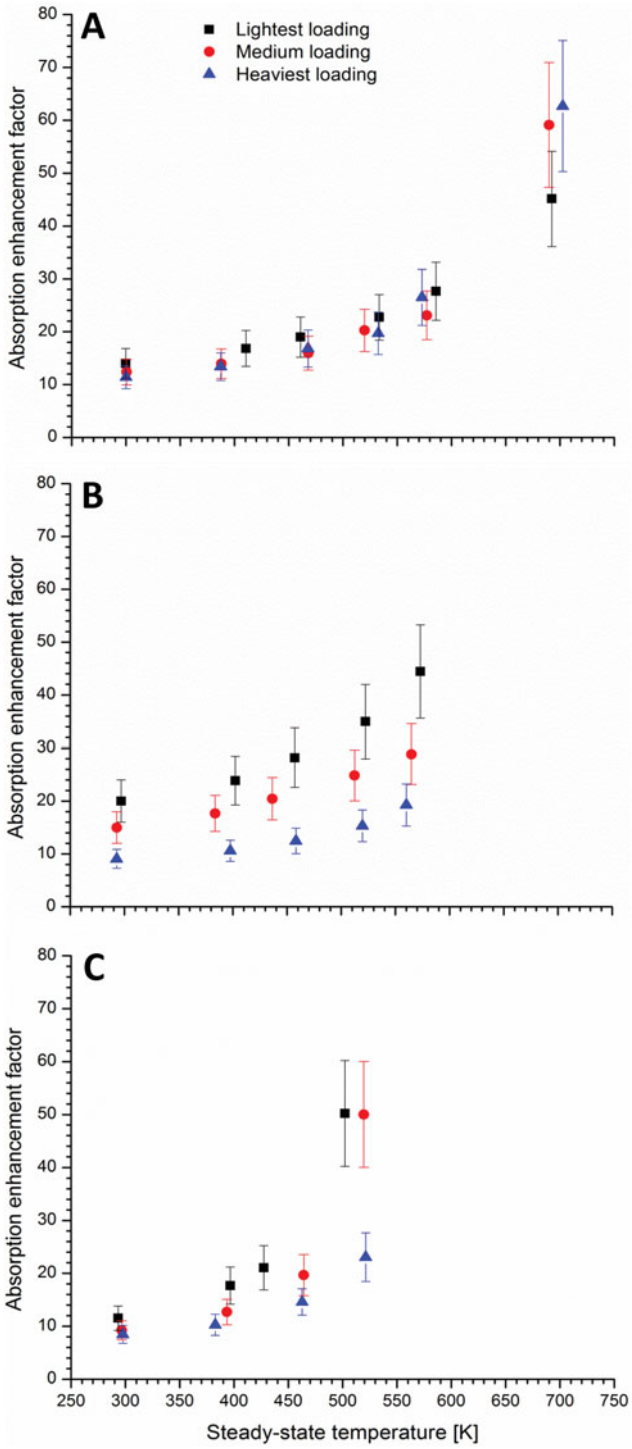

FIG. 8. Variation of nigrosin absorption enhancement factor (α_R) with steady-state sample temperature (T_o) at different particle mass loadings for (a) quartz, (b) Zefluor, and (c) Zylon filter materials.

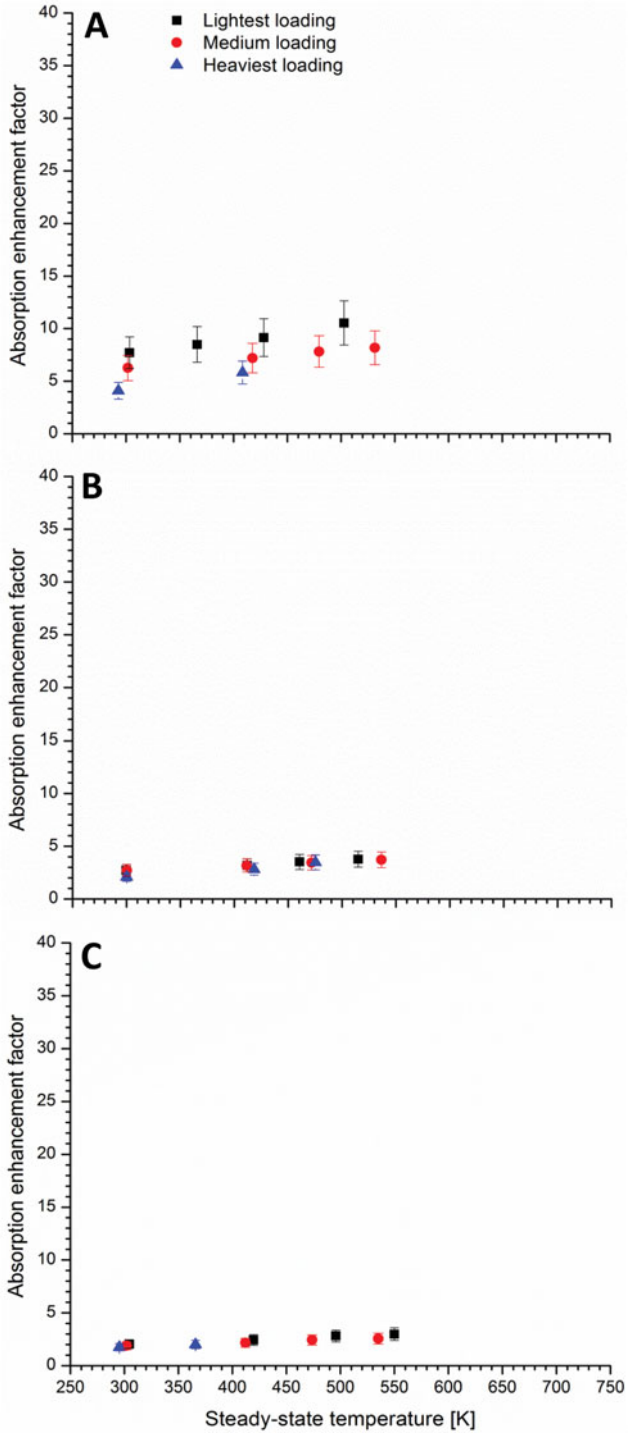

FIG. 9. Variation of nigrosin absorption enhancement factor (α_R) with steady-state sample temperature (T_o) at different particle mass loadings for nuclepore filter materials with (a) 1 μm, (b) 5 μm, and (c) 10 μm pore sizes.

increasing steady-state sample temperature (i.e., increased laser radiation) is again attributed to the increased filter-surface scattering and enhanced particle absorption for the nigrosin-laden filter, as opposed to the isolated nigrosin. Comparing filter types, the results for the quartz substrate are similar to that for the Zylon. Comparing the Teflon filters, the smaller-pore-size Zefluor filter results in larger absorption enhancement ratios than the larger-pore-size Zylon filter (Figure 8), which may be related to the observed clogging of the larger pores (i.e., shadowing effect). Similarly, when comparing the three polycarbonate filters, again the value of α_R decreases as the pore size increases (Figure 9).

Regarding particle deposition within the fibers of quartz fibrous filters, the particle size distribution was not monodisperse during deposition, and the flow velocity was not varied (for equivalent particle loadings) to achieve greater penetration into the fibers. These effects were reported by Moteki et al. (2010), and Nakayama et al. (2010) for which size-dependent correction factors in fibrous filters were established for PSAP. In this investigation, the flow rate was kept unchanged for a particular filter; the loading was varied by changing the particle-collection time. Thus, one can assume similar penetration depths for the investigated quartz fibrous filters. Perhaps this explains, in part, the difference in the larger absorption enhancement ratio for the quartz fibrous filter, as compared to the reported literature values (i.e., having lower values due to shadowing effects of the penetrated particles). The nigrosin size distribution was also measured using dynamic light scattering and compared with Lorenz–Mie calculations (Presser 2012). For the membrane polycarbonate filters, there is no surface penetration; coating and clogging of the pores (i.e., by deposition of larger particles, faster flow rates, and higher particle densities) are the parameters that influence absorption enhancement or shadowing effects. The difference in the surface penetration between the fibrous and membrane filters may explain why the absorption enhancement effect is less for the membrane filters.

As described earlier, the mass-specific absorption cross-section is sensitive to shadowing effects (for heavier filter loadings). This is to be expected since the absorbance is dependent on the mass-specific absorption cross-section (Equation (1)). As shown in Collaud Coen et al. (2010), shadowing affects the absorbance and is corrected either empirically (Weingartner et al. 2003) or with theoretical considerations of the total optical depth (i.e., from the filter transmission) (Arnott et al. 2005). It is suggested that shadowing be corrected either empirically through the mass-specific absorption cross-section since it should be independent of the mass loading), or by theoretically estimating the absorption penetration depth (see Equation (13) in Presser 2012) beyond which particles will not be contributing to absorption.

5. SUMMARY

The absorption coefficient and mass-specific absorption cross-section for different steady-state temperatures and particle mass loadings were determined for quartz, Teflon, and polycarbonate filter materials. Quartz is a fibrous material while Teflon and polycarbonate are porous; the effect of pore size was also studied for the porous substrates. The substrates were coated with nigrosin, which has been used in several prior investigations

found in the literature. To determine the absorption coefficient, the absorptivity was obtained from a new rapid laser-heating technique and the transmissivity was obtained from classical transmission measurements. This technique was used to isolate the absorption properties of the particle coating from the substrate, and investigate substrate effects on enhancing absorption in terms of a defined absorption enhancement ratio. The results indicated that the isolated-nigrosin absorption coefficient increased with nigrosin mass loading and decreased with steady-state temperature. The isolated-nigrosin absorption coefficient also increased with pore size for the porous filters (which was attributed to the accumulation and thicker deposit of particles at the pores). The isolated-nigrosin, mass-specific absorption cross-section was not found to be independent of the mass loading, but was found to decrease with increasing particle concentration. This result is attributed to shadowing effects, for which particle obscuration by other particles results in reduced absorption. The effects of the filter substrate on enhancing absorption tends to be more significant for increasing steady-state temperature, lighter mass loadings, and for filter substrates with smaller pore sizes. The values of the absorption enhancement ratio varied widely among the different filter materials with the effect by the Zefluor filter being the most significant and polycarbonate filters being similar to values found in the literature.

This study provides another independent methodology for determining aerosol absorption characteristics and comparing results with established techniques to enhance measurement confidence. For filter-based aerosol absorption methods, one may consider (1) evaluating absorption directly, with a more detailed theoretical formulation, to avoid the complexities of a scattering measurement, (2) removing the filter contribution in the theoretical analysis in order to isolate particle absorption, enable comparison with the particle-laden filter, and estimate absorption enhancement effects, and (3) using the mass-specific absorption cross-section to evaluate shadowing effects.

ACKNOWLEDGMENTS

The authors thank Mr. M. Jones for his assistance while participating as a NIST Summer Undergraduate Research Fellow.

SUPPLEMENTAL MATERIAL

Supplemental data for this article can be accessed on the publisher's website.

REFERENCES

Arnott, W. P., Hamasha, K., Moosmuller, H., Sheridan, P. J., and Ogren, J. A. (2005). Towards Aerosol Light Absorption Measurements with a 7-Wavelength Aethalometer: Evaluation with a Photoacoustic Instrument and a 3-Wavelength Nephelometer. *Aerosol Sci. Technol.*, 39(1):17–29.

Baker, R.W. (2004). *Membrane Technology and Applications* (2nd ed.), Wiley, New York, pp. 66–68, 92–94.

Baumgardner, D., Popovicheva, O., Allan, J., Bernardoni, V., Cao, J., Cavalli, F., et al. (2012). Soot Reference Materials for Instrument Calibration and Intercomparisons: A Workshop Summary with Recommendations. *Atmos. Meas. Tech.*, 5(8):1869–1887.

Birch, M. E., and Cary, R. A. (1996). Elemental Carbon-Based Method for Monitoring Occupational Exposures to Particulate Diesel Exhaust. *Aerosol Sci. Technol.*, 25(3):221–241.

Bohren, C. F., and Huffman, D. R. (1983). *Absorption and Scattering of Light by Small Particles*, Wiley, New York, pp. 28–41, 77–81.

Bond, T. C., Anderson, T. L., and Campbell, D. (1999). Calibration and Intercomparison of Filter-Based Measurements of Visible Light Absorption by Aerosols. *Aerosol Sci. Technol.*, 30(6):582–600.

Bond, T. C., and Bergstrom, R. W. (2006). Light Absorption by Carbonaceous Particles: An Investigative Review. *Aerosol Sci. Technol.*, 40(1):27–67.

Bond, T. C., Doherty, S. J., Fahey, D. W., Forster, P. M., Berntsen, T., DeAngelo, B. J., et al. (2013). Bounding the Role of Black Carbon in the Climate System: A Scientific Assessment. *J. Geophys. Res.: Atmospheres*, 118(11):5380–5552.

Brinkworth, B. J. (1972). Interpretation of the Kubelka-Munk Coefficients in Reflection Theory. *Appl. Opt.*, 11(6):1434–1435.

Bruce, C. W., Stromberg, T. F., Gurton, K. P., and Mozer, J. B. (1991). Trans-Spectral Absorption and Scattering of Electromagnetic Radiation by Diesel Soot. *Appl. Opt.*, 30(12):1537–1546.

Campbell, D., Copeland, S., and Cahill, T. (1995). Measurement of Aerosol Absorption Coefficient from Teflon Filters using Integrating Plate and Integrating Sphere Techniques. *Aerosol Sci. Technol.*, 22(3):287–292.

Cappa, C. D., Lack, D. A., Burkholder, J. B., and Ravishankara, A. R. (2008). Bias in Filter-Based Aerosol Light Absorption Measurements due to Organic Aerosol Loading: Evidence from Laboratory Measurements. *Aerosol Sci. Technol.*, 42(12):1022–1032.

Chow, J. C., Watson, J. G., Pritchett, L. C., Pierson, W. R., Frazier, C. A., and Purcell, R. G. (1993). The DRI Thermal/Optical Reflectance Carbon Analysis System: Description, Evaluation and Applications in US Air Quality Studies. *Atmos. Environ.*, 27A(8):1185–1201.

Clarke, A. D. (1982). Effects of Filter Internal Reflection Coefficient on Light Absorption Measurements Made Using the Integrating Plate Method. *Appl. Opt.*, 21(16):3021–3031.

Collaud Coen, M., Weingartner, E., Apituley, A., Ceburnis, D., Fierz-Schmidhauser, R., Flentje, H., et al. (2010). Minimizing Light Absorption Measurement Artifacts of the Aethalometer: Evaluation of Five Correction Algorithms. *Atmos. Meas. Tech.*, 3(2):457–474.

Conny, J. M., Klinedinst, D. B., Wight, S. A., and Paulsen, J. L. (2003). Optimizing Thermal-Optical Methods for Measuring Atmospheric Elemental (Black) Carbon: A Response Surface Study. *Aerosol Sci. Technol.*, 37(9):703–723.

Conny, J. M. (2007). The Optimization of Thermal Optical Analysis for the Measurement of Black Carbon in Regional PM2.5: A Chemometric Approach. EPA Report 600/R-07/119, U.S. EPA, Research Triangle Park, NC.

Conny, J. M., Norris, G. A., and Gould, T. R. (2009). Factorial-Based Response-Surface Modeling with Confidence Intervals for Optimizing Thermal-Optical Transmission Analysis of Atmospheric Black Carbon. *Analytica Chimica Acta*, 635(2):144–156.

Fry, E. S., Kattawar, G. W., and Pope, R. M. (1992). Integrating Cavity Absorption Meter. *Appl. Opt.*, 31(12):2055–2065.

Fuller, K. A., Maim, W. C., and Kreidenweis, S. M. (1999). Effects of Mixing on Extinction by Carbonaceous Particles. *J. Geophys. Res.: Atmospheres*, 104(D13):15,941–15,954.

Hänel, G. (1987). Radiation Budget of the Boundary Layer: Part II. Simultaneous Measurement of Mean Solar Volume Absorption and Extinction Coeffcients of Particles. *Beiträge zur Physik der Atmosphäre*, 60:241–247.

Hänel, G. (1994). Optical Properties of Atmospheric Particles: Complete Parameter Sets Obtained Through Polar Photometry and an Improved Inversion Technique. *Appl. Opt.*, 33(30):7187–7199.

Hansen, A. D. A., Rosen, H., and Novakov, T. (1984). The Aethalometer—An Instrument for the Real-Time Measurement of Optical Absorption of Aerosol Particles. *Sci. Total Environ.*, 36:191–196.

Hitzenberger, R. (1993). Absorption Measurements with an Integrating Plate Photometer Calibration and Error Analysis. *Aerosol Sci. Technol.*, 18(1):70–84.

Hitzenberger, R., Dusek, U., and Berner, A. (1996). Black Carbon Measurement Using an Integrating Sphere. *J. Geophys. Res.: Atmospheres*, 101(D14):19,601–19,606.

Horvath, H. (1993). Comparison of Measurements of Aerosol Optical Absorption by Filter Collection and a Transmissometric Method. *Atmos. Environ.*, 27A(3):319–325.

Horvath, H. (1997). Experimental Calibration for Aerosol Light Absorption Measurements Using the Integrating Plate Method—Summary of the Data. *Aerosol Sci.*, 28(7):1149–1161.

Incropera, F.P., and DeWitt, D.P. (2001). *Introduction to Heat Transfer* (4th ed.), Wiley, New York, 248, 516, and 662–663.

Justus, B. L., Kafafi, Z. H., and Huston, A. L. (1993a). Excited-State Absorption-Enhanced Thermal Optical Limiting in C_{60}. *Opt. Lett.*, 18(19):1603–1605.

Justus, B. L., Huston, A. L., and Campillo, A. J. (1993b). Broadband Thermal Optical Limiter. *Appt. Phys. Lett.*, 63(11):1483–1485.

Kirchstetter, T. W., and Novakov, T. (2007). Controlled Generation of Black Carbon Particles from a Diffusion Flame and Applications in Evaluating Black Carbon Measurement Methods. *Atmos. Environ.*, 41(9):1874–1888.

Kondo, Y., Sahu, L., Kuwata, M., Miyazaki, Y., Takegawa, N., Moteki, N., et al. (2009). Stabilization of the Mass Absorption Cross Section of Black Carbon for Filter-Based Absorption Photometry by the Use of a Heated Inlet. *Aerosol Sci. Technol.*, 43(8):741–756.

Kondo, Y., Sahu, L., Moteki, N., Khan, F., Takegawa, N., Liu, X., et al. (2011). Consistency and Traceability of Black Carbon Measurements Made by Laser-Induced Incandescence, Thermal-Optical Transmittance, and Filter-Based Photo-Absorption Techniques. *Aerosol Sci. Technol.*, 45(2):295–312.

Lack, D. A., Lovejoy, E. R., Baynard, T., Pettersson, A., and Ravishankara, A. R. (2006). Aerosol Absorption Measurement Using Photoacoustic Spectroscopy: Sensitivity, Calibration, and Uncertainty Developments. *Aerosol Sci. Technol.*, 40(9):697–708.

Lawless, P. A., Rodes, C. E., and Ensor, D. S. (2004). Multiwavelength Absorbance of Filter Deposits for Determination of Environmental Tobacco Smoke and Black Carbon. *Atmos. Environ.*, 38(21):3373–3383.

Lodge, J. P., Jr. (1989). *Methods of Air Sampling and Analysis* (3rd ed.), Lewis Publishing, Michigan.

Mogo, S., Cachorro, V. E., and de Frutos, A. M. (2005). Morphological, Chemical and Optical Absorbing Characterization of Aerosols in the Urban Atmosphere of Valladolid. *Atmos. Chem. Phys. Discuss.*, 5(3):3921–3957.

Moosmüller, H., Arnott, W. P., Rogers, C. F., Chow, J. C., and Frazier, C. A. (1998). Photoacoustic and Filter Measurements Related to Aerosol Light Absorption During the Northern Front Range Air Quality Study (Colorado 1996/1997). *J. Geophys. Res.: Atmospheres*, 103(D21):28,149–28,157.

Moosmüller, H., Chakrabarty, R. K., and Arnott, W. P. (2009). Aerosol Light Absorption and Its Measurement: A Review. *J. Quantitative Spectroscopy and Radiative Transfer*, 110(11):844–878.

Moteki, N., Kondo, Y., Nakayama, T., Kita, K., Sahu, L.K., Ishigai, T., et al. (2010). Radiative Transfer Modeling of Filter-Based Measurements of Light Absorption by Particles: Importance of Particle Size Dependent Penetration Depth. *J. Aerosol Sci.*, 41(4):401–412.

Nakayama, T., Kondo, Y., Moteki, N., Sahu, L.K., Kinase, T., Kita, K., et al. (2010). Size-Dependent Correction Factors for Absorption Measurements Using Filter-Based Photometers: PSAP and COSMOS. *J. Aerosol Sci.*, 41(4):333–343.

Nazarian, A., and Presser, C. (2008). Thermal and Chemical Kinetic Characterization of Multiphase and Multicomponent Substances by Laser Heating. *Int. J. Heat Mass Transfer*, 51(5–6):1365–1378.

Ogren, J. A. (2010). Comment on "Calibration and Intercomparison of Filter-Based Measurements of Visible Light Absorption by Aerosols". *Aerosol Sci. Technol.*, 44(8):589–591.

Petzold, A., and Schönlinner, M. (2004). Multi-Angle Absorption Photometry—A New Method for the Measurement of Aerosol Light Absorption and Atmospheric Black Carbon. *J. Aerosol Sci.*, 35(4):421–441.

Petzold, A., Schloesser, H., Sheridan, P. J., Arnott, W. P., Ogren, J. A., and Virkkula, A. (2005). Evaluation of Multiangle Absorption Photometry for Measuring Aerosol Light Absorption. *Aerosol Sci. Technol.*, 39(1):40–51.

Petzold, A., Ogren, J. A., Fiebig, M., Laj, P., Li, S.-M., Baltensperger, U., et al. (2013). Recommendations for Reporting "Black Carbon" Measurements. *Atmos. Chem. Phys.*, 13(16):8365–8379.

Presser, C. (2012). Absorption Coefficient Measurements of Particle-Laden Filters Using Laser Heating: Validation with Nigrosin. *J. Quantitative Spectroscopy and Radiative Transfer*, 113(8):607–623.

Radney, J. G., Bazargan, M. H., Wright, M. E., and Atkinson, D. B. (2009). Laboratory Validation of Aerosol Extinction Coefficient Measurements by a Field-Deployable Pulsed Cavity Ring-Down Transmissometer. *Aerosol Sci. Technol.*, 43(1):71–80.

Sadler, M., Charlson, R. J., Rosen, H., and Novakov, T. (1981). An Intercomparison of the Integrating Plate and the Laser Transmission Methods for Determination of Aerosol Absorption Coefficients. *Atmos. Environ.*, 15(7):1265–1268.

Schmid, O., Artaxo, P., Arnott, W. P., Chand, D., Gatti, L. V., Frank, G. P., et al. (2006). Spectral Light Absorption by Ambient Aerosols Influenced by Biomass Burning in the Amazon Basin. I: Comparison and Field Calibration of Absorption Measurement Techniques. *Atmos. Chem. Phys.*, 6(11):3443–3462.

Sedlacek, A., and Lee, J. (2007). Photothermal Interferometric Aerosol Absorption Spectrometry. *Aerosol Sci. Technol.*, 41(12):1089–1101.

Sheridan, P. J., Arnott, W. P., Ogren, J. A., Andrews, E., Atkinson, D. B., Covert, D. S., et al. (2005). The Reno Aerosol Optics Study: An Evaluation of Aerosol Absorption Measurement Methods. *Aerosol Sci. Technol.*, 39(1):1–16.

Siegel, R., and Howell, J. R. (1981). *Thermal Radiation Heat Transfer* (2nd ed.), Hemisphere, New York, Chapters 13 and 19.

Subramanian, R., Roden, C. A., Boparai, P., and Bond, T. C. (2007). Yellow Beads and Missing Particles: Trouble Ahead for Filter-Base Absorption Measurements. *Aerosol Sci. Technol.*, 41(6):630–637.

Taha, G. Box, G. P., Cohen, D. D., and Stelcer, E. (2007). Black Carbon Measurement using Laser Integrating Plate Method. *Aerosol Sci. Technol.*, 41(3):266–276.

Taylor, B. N., and Kuyatt, C. E. (1994). Guidelines for Evaluating and Expressing the Uncertainty of NIST Measurement Results. NIST Technical Note 1297, National Institute of Standards and Technology, Gaithersburg, MD.

Virkkula, A., Ahlquist, N. C., Covert, D. S., Arnott, W. P., Sheridan, P. J., Quinn, P. K., et al. (2005). Modification, Calibration and a Field Test of an Instrument for Measuring Light Absorption by Particles. *Aerosol Sci. Technol.*, 39(1):68–83.

Virkkula, A., Makela, T., Hillamo, R., Yli-Tuomi, T., Hirsikko, A., Hameri, K., et al. (2007). A Simple Procedure for Correcting Loading Effects of Aethalometer Data. *J. Air Waste Manage*, 57(10):1214–1222.

Virkkula, A. (2010). Correction of the Calibration of the 3-Wavelength Particle Soot Absorption Photometer (3λ PSAP). *Aerosol Sci. Technol.*, 44(8):706–712.

Weingartner, E., Saathoff, H., Schnaiter, M., Streit, N., Bitnar, B., and Baltensperger, U. (2003). Absorption of Light by Soot Particles: Determination of the Absorption Coefficient by Means of Aethalometers. *J. Aerosol Sci.*, 34(10):1445–1463.